International Journal of Aviation, Aeronautics, and Aerospace

Volume 2 | Issue 1 Article 2

3-2-2015

Comparison of Aircraft Tire Wear with Initial Wheel Rotational Speed

Abdurrhman A. Alroqi
University of Sussex, aa-alroqi@hotmail.com
Weiji Wang
University of Sussex, w.j.wang@sussex.ac.uk

Comparison of Aircraft Tire Wear with Initial Wheel Rotational Speed

Cover Page Footnote
The authors would like to acknowledge University of Sussex for its support with the literature and related resources.

In this paper, the landing impact of an aircraft is described using a physical model of a single wheel in the main landing gear. The purpose of this study is to understand potential tire-life improvements that could be made by reducing abrasive skidding between aircraft tires and runway surfaces immediately after touchdown.

The physical model assumes the following chain of events during a typical landing: Firstly, the landing gear is extended during the aircraft approach towards the runway. The main wheels first contact the ground while the wheels are not spinning at ground-speed. A difference between the translational ground-speed of the aircraft and the tangential speed of the tire radius results in a skid which reduces in severity as the wheels accelerate to match the forward speed of the aircraft along the runway. A small cloud of smoke is often visible following the initial touchdown. The cause of landing smoke has been identified as resulting from high friction between the tire and runway surfaces (Cadle & Williams, 1978). This friction generates significant heat, which can trigger burning of the softer surface (Tomita, 1964). The softer surface is the tire tread, which for civilian aircraft is made of nearly 100% natural rubber (Hunter, 1997), which has highly elastic dynamic properties and high resistance to heat (De & White, 2001).

The main landing gear of a Boeing 747-400 is modelled as a one-dimensional mass-spring-damper system for analysis of forces during the short period between touchdown and the wheels spinning up to match the ground speed of the aircraft. Distinct dynamic states of the tire during landing have been identified in this case study: touchdown, traction-limited skidding, tire spin-up and free rolling.

Literature Review

Literature describing the physical process that causes aircraft tire rubber to vaporize under landing loads is sparse, although multiple studies have been reported in the automotive field. Tire skid-marks are caused by material being removed by abrasion between slipping tires and the asphalt runway surface. Persson (2006) states that the friction force generated between the tire and asphalt surfaces is related to the internal friction of the rubber, which is a bulk property. The hysteretic friction component is determined by gripping and sliding of the rubber over a rough surface. These oscillating forces lead to energy dissipation, which can cause heating of the tire material to a level where smoke is produced.

Few studies were found to have attempted simulation modelling of longitudinal tire dynamics during landings. In the first, Padovan, Kazempour and Kim (1990) built an energy-balance model to compute the rate of work due to interfacial friction between tire and runway surfaces and its effect on

the growth of wheel rotary inertia and slip work. In the study, calculations were based on a model of the space-shuttle, which experiences a large amount of tire wear per landing. A simple Coulomb-friction formulation $F_X = \mu F_R$ tire friction model was employed, using a constant friction coefficient μ and a non-linear curve fitted to experimental data to express vertical tire load F_R. Padovan, Kazempour and Kim (1990) concluded from various simulations that tire wear was increased with horizontal landing speed, sink rate and surface friction coefficients.

Slagmaat (1992) investigated suitable tire models for simulating longitudinal aircraft tire dynamics and found the Pacejka "magic formula" models, popular in automotive literature, were not suitable to represent the fast-dynamics in aircraft landings. Significant simplifications were applied to the Pacejka tire model in (Slagmaat, 1992), and a multi-body nonlinear landing gear model was implemented for vertical tire-load simulation, although comparisons with experimental results were not made due to a lack of reliable experimental data being available.

In (Li & Jiao, 2013), a simulation model was built for an anti-lock braking system (ABS) to be used on large aircraft. The highly dynamic tire forces were successfully modeled in that study with the use of a modern LuGre tire model.

Besselink (2000) produced a sophisticated model for simulating lateral "shimmy" oscillations in main landing gear of a Boeing 747-400 aircraft. Although the scope of this work does not involve lateral dynamics, some important experimental data was recorded, including experimental wheel-speed time traces measured on a Boeing 747-400 aircraft during landing, which are useful for validating our simulations. Measured data in both Besselink (2000) and Khapane (2004) show aircraft tires accelerating from zero rotational speed to a free-rolling velocity within about 0.1 seconds from touchdown.

However, some example aircraft wheel spinner patents designed to prevent the aircraft landing smoke are presented here. No valid proof of the systems that those patents define validated to eliminate landing smoke and tire wear arose in the literature review, and to our knowledge no aircraft industries use these patents. Aircraft landings continue to generate smoke, a screeching sound, flat spots on tires, and the need to periodically replace the tires; indicating a significant issue that is addressed in this paper. Patented solutions have been suggested by Beazley (1947) and others. The benefits of a successful design include longer tire life, improved landing safety, reduced parts fatigue and maintenance costs, less tarmac rubber-cleaning, a lower risk of tire blow-outs, and a lower risk of tire debris being ingested into jet engines. Additionally, there are environmental benefits such as reduction of tire smoke,

DOI: https://doi.org/10.15394/ijaaa.2015.1043

noise, and air pollution caused by the disintegrating tires (Beazley, 1947). As a result, various ideas have circulated since as early as the 1940s, several of which are presented here.

Patents for aircraft wheel rotational devices and methods focus on ideas that range from the simple to mechanically complex. The literature indicates that some pre-rotating systems are mechanically complex, heavy, or not durable. Therefore, several patents focus on passive air flow systems that require modifications to the wheels themselves to cause the air stream to rotate the descending wheels before they touch the ground. Most of these are wheel-mounted accessories intended to utilize the air stream during descent to start aircraft tires rotating before touchdown, while others are complex systems utilising magnetic, hydraulics, compressed air and gas, and other mechanical systems.

Pre-rotation is the primary means of getting tires on an airborne plane to begin spinning before they hit the tarmac on landing. Khal and Khal (2013), utilize a flap system made of a flexible resin plastic base, then Kevlar-type material, then a top layer of similar material as the base, all bonded together with stitching, adhesive, and/or thermoplastic bonding. Each disc-shaped piece has passive, auto-retracting flaps or vanes that open when exposed to the air stream created by the descending plane. Above the horizontal centreline of the wheel, the hinged flap leads into wind and the flaps close; below the tire's centreline, air pushes the flaps open and fully open at the bottom; this torque is aerodynamically generated, forcing the wheel into rotation. Additional structures keep the flap from exceeding 90 degrees when open. One complication of operating this device is that the outer circumference of the disc may include a weighted ring to supply centrifugal force to reset a disc displaced by a rough landing, bolting into the tires themselves may compromise their inherent structure. Thus, this assembly does not appear to be as viable a design as some others.

Horvath and Szoke (2006), avoid the addition of an assembly to the wheel and instead alter the tire’s design to incorporate curved air foils that protrude from both sides of each tire. Placing the foils on both sides, it is claimed, will minimize protrusion. The inventors suggest the foils could also be attached to existing tires and made of “durable material”, suggesting rubber, synthetic rubber, and closed or open cell foam. This material can then be bonded to “the carcass plies by nylon fabric or other methods, and covered by rubber or other synthetic materials”. While there is a potentially good concept, Horvath and Szoke have not executed their idea in real-world testing. Moreover, such a tire design change would likely also require all new wheel assemblies and enclosures to accommodate them, which is neither cost effective nor feasible.

Numerous inventions have been registered to pre-spin aircraft tires before touchdown, although none of the patents researched mentioned any estimate on expected improvements on tire life. The goal of this study is to predict the difference in tire wear between pre-spun and un-spun aircraft wheels.

Simulation Model

The following subsections describe physical relationships used in the development of a Simulink model that is used to predict the forces acting on a tire during a typical landing event, and also predict the tire wear with different initial conditions.

The following assumptions (with the support of references) were used to simplify calculations.

- The pilot does not brake during the spin-up phase after touchdown. This avoidance of immediate brake use avoids locked wheels, increased skidding, and a tire flat spot that leads to more tire and brake pad wear (United states air force, 2007).
- The aircraft will touchdown with all of the main wheels and zero wing lift (Jingzhe, 2007) and (Daidzic & Shrestha , 2008); the landing is smooth with an acceptable sink rate (vertical speed) to be absorbed by the shock absorbers and tires. Additionally, the nose wheel will not touch the ground for two seconds after the main wheels. This latter assumption is because the aircraft may touchdown on the runway with some lift still generated by the wing, and the aircraft weight will not be applied equally to all wheels simultaneously because it might be affected by cross wind, and pilot action. Furthermore, the aircraft may land on one wheels leg, which leads to hard landing and strong forces applied to the wheels (FAA, 2004).
- Static friction coefficients of the tire and runway materials are constant throughout the landing process, and a Lugre tire model (Canudas-de-Wit, Tsiotras, Velenis, Basset & Gissinger, 2003) is used to determine the dynamic friction forces acting friction.
- Shock absorbers in the landing gear structure absorb the majority highly dynamic vertical forces, and tire deflection is assumed to vary linearly with vertical load according to a spring law.
- Wheel spin-up or “skid” time is the measured time between touchdown and the landing gear wheels reaching a steady speed that matches the ground speed of the aircraft.

Landing Gear Dynamics

The mass-spring-damper system depicted in Figure 1 was used to model vertical forces acting on the aircraft mass and tires contact patch. The

DOI: https://doi.org/10.15394/ijaaa.2015.1043

landing gear dynamics model architecture is practically identical to the model presented in (Lernbeiss, 2004), and (Tanyolac & Yasarcan, 2011).

F_z represents the downward force reacted by the landing gear structure, and is equal to aircraft weight minus lift. Because zero lift is assumed from the moment of touchdown (Jingzhe, 2007), and (Daidzic & Shrestha , 2008), F_z is simply the aircraft weight. Balancing forces vertically, the equation representing oscillation of the vehicle mass in Figure 1 is:

$$F_z = m\ddot{z} + c\dot{z} + kz, \quad (1)$$

Where m represents the vehicle mass, c is the damping coefficient of the landing gear's shock-absorbers (Ns/m), k is the linear stiffness of the landing gear suspension (N/m), and z is the vertical displacement of the lumped aircraft mass (m). The datum for z is initialised with a value of zero at the moment of touchdown. $\dot{z}$ is the vertical velocity of aircraft body (sink rate) (m/s), and $\ddot{z}$ is the vertical acceleration of aircraft body from touchdown (m/s^2).

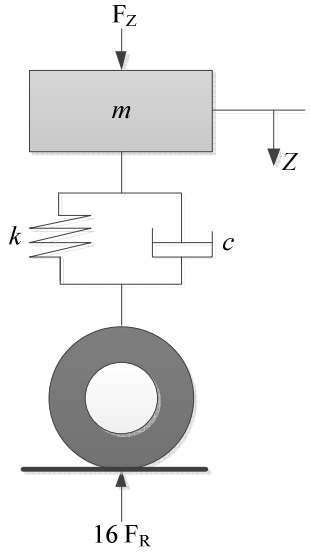

Figure 1. Mass-spring-damper system used to model vertical forces on the landing gear structure.

From inspection of the system in Figure 1 and (eq. 1), the vertical force reacted over the tire contact patches of *all 16 wheels* in the main gear is:

$$16F_R = c\dot{z} + kz \quad (2)$$

Equations (1) & (2) show that in a static condition the vertical force reacted by the tire is equal to the landing gear spring-constant multiplied by the displacement in suspension springs, which is also equal to aircraft weight.

The damping term *c* in (eq. 2) shows the vertical force acting on the tire at the instant of touchdown will be larger at higher sink rates, i.e. the vertical velocity at which the wheel initially hits the ground.

The combined spring constant for the main landing gear of a Boeing 747-400 (four oleo struts in parallel) is 5×10^6 N/m and the damping coefficient of the landing gear shock absorber is 5.473×10^6 Ns/m (Jingzhe, 2007). The aircraft mass is 295,743 kg (Boeing, 2011), so in a static condition the force F_R is equal to 181.33 kN ($mg/16$).

Wheel Geometry

The wheels are assumed to start to spin up from zero rotational speed when the aircraft lands until they reach the aircraft forward speed, and then decelerate as the aircraft decelerates. Figure 2 shows the rigid wheel forces at the moment of touchdown ($t = 0$).

The wheel radius, R, will deflect under the aircraft weight to become the deflection radius, r_d. The amount of the deflection is $\delta\ (= \mathrm{DB})$. The arc ADC will be the tire footprint ABC when it is compressed. The vertical force acting downwards on a single wheel is $\mathrm{F_z}/16$ because the main landing gear has 16 wheels. That force gives rise to an immediate friction force $F_x(= \mu F_R)$, where F_R is the reaction force to the weight on the wheel. The aircraft landing speed on the runway, v, and the angular displacement of the wheel, $\emptyset$, are shown. Geometric relationships from (Milwitzky, Lindquist & Potter, 1955) follow.

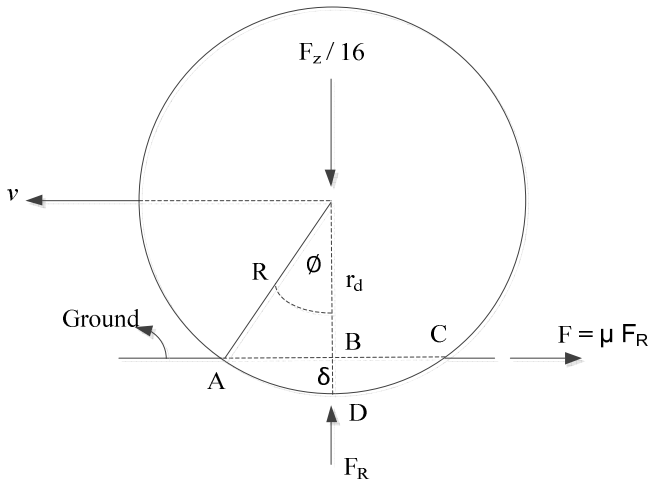

Figure 2. The forces on wheel in contact with runway. From Milwitzky, Lindquist & Potter, 1955.

The tire deflection shown Figure 2 is defined by:

$$r_d = R - \delta \tag{3}$$

DOI: https://doi.org/10.15394/ijaaa.2015.1043

If there was enough slip across the extent of the tire contact patch then the tire might rotate as if the true radius were the geometric value of the axle height r_d. However, this is not the case for a generalized pneumatic tire with bias-ply construction, although an effective radius r_e can be used, as in (Daugherty, 2003) which generalizes the rolling radius across the tire contact patch AC.

From trigonometry the angular displacement between the center and edge of the contact patch is:

$$\emptyset = \sin^{-1}\frac{\sqrt{R^2 - {r_d}^2}}{R} \tag{4}$$

And the horizontal translation of rolling is:

$$AB = \sqrt{\mathrm{R}^2 - {\mathrm{r}_d}^2} \tag{5}$$

Combining (eq. 4) with (eq. 5) yields the effective rolling radius;

$$r_e = \frac{AB}{\emptyset} = \frac{\sqrt{\mathrm{R}^2 - {\mathrm{r}_d}^2}}{\sin^{-1}\frac{\sqrt{R^2 - {r_d}^2}}{R}} = \frac{R\sqrt{1 - \frac{{\mathrm{r}_d}^2}{\mathrm{R}^2}}}{\sin^{-1}\sqrt{1 - \frac{{\mathrm{r}_d}^2}{\mathrm{R}^2}}} \tag{6}$$

Proof in (Milwitzky, Lindquist & Potter, 1955) concludes that the right-hand side of (eq. 6) is closely approximated by the linear function $\frac{2R + r_d}{3}$, so that:

$$r_e \approx \frac{2R + r_d}{3} \tag{7}$$

or, since $r_d = R - \delta$ from (eq. 3) ,

$$r_e = R - \frac{\delta}{3} \ . \tag{8}$$

The tire deflection can be calculated by modeling linear deflection from deflection vs. load data in (Lindsley & Talekar, 2000) with a spring constant of $k_t = 1.7x10^6$ meters per Newton vertical load ($k_t = F_R/\delta$), which gives a constant effective tire rolling radius of 0.586 m when the aircraft is in a static condition. Tire geometry data is given in Table 2.

LuGre Tire/Road Friction Model

The LuGre model was selected for use in preference to static brush models (Bartram, Mavros, & Biggs, 2010) for the LuGre model's ability to capture fast dynamic conditions. The dynamic Dahl model (Dahl, 1968) is

unable to model the Stribeck effect, which describes sticking and slipping motion, whereas LuGre model can. The LuGre tire model only requires 6 input parameters (given in Table 1), unlike Pacejka models which can require a vast amount of curve-fitting parameters to which the force output can be sensitive (Hamza, 2014). As explained by (Slagmaat, 1992), the Pacejka "magic formula" is not a first order differential equation like conventional tire models, but an algebraic equation simply fitted to steady-state observations. The lack of dependence on time-derivatives results in less accurate predictions if transient behavior is of interest. Another reason for not choosing the "magic formula", which is popular in automotive literature, as computational tire model is the lack of appropriate parameter values for aircraft tires. Parameters in Pacejka's "magic formula" form curve fittings of force coefficients from measurements under varying normal loads. The range of aircraft tire normal loads is up to fifteen times wider than typical automotive tire loads and starts from zero, rendering car tire curve fittings invalid in most of the used range in the aircraft tire.

The longitudinal friction force F_X that acts at the tire contact point and acts to accelerate the wheel rotationally is modeled using the LuGre tire model described by (Li & Jiao, 2013).

The aircraft tire/runway friction coefficient is defined by the ratio of friction force and the normal force, which can be expressed as:

$$\mu = \frac{F_x}{F_R} \tag{9}$$

where the friction coefficient μ is a complex function of the aircraft longitudinal slip and other factors, such as tire and runway conditions.

Longitudinal slip between a point on the tire's outer radius and the ground is defined by:

$$\lambda = \frac{v - r_e\omega}{v} \tag{10}$$

where v is the aircraft's forward speed along the runway and ω is the rotational speed of the wheel in radians per second.

The LuGre tire model formulation is based on a distribution of longitudinal and normal forces distributed within the tire contact patch (Canudas-de-Wit, Tsiotras, Velenis, Basset & Gissinger, 2003) although, as demonstrated in (ESDU, 1995), the lumped LuGre model is a good approximation of the distributed LuGre model, as they have similar steady-state and dynamic behavior.

DOI: https://doi.org/10.15394/ijaaa.2015.1043

Frictional forces in the LuGre model depend upon evolution of the mean internal friction state $\tilde{z}$, which is effectively the average stretched displacement of rubber across the tire contact patch. The internal friction state within the contact patch, from (Canudas-de-Wit, Petersen & Shiriaev, 2003) is defined by the differential equation:

$$\frac{d\tilde{z}}{dt} = v_r - \frac{\sigma_0|v_r|}{g(v_r,v_s)}\tilde{z} \tag{11}$$

Where σ_0 is the normalized tire stiffness, and v_r is the relative speed between a point tangential to the outer tire surface and the forward speed of the aircraft along the runway:

$$v_r = v - r_e\omega \tag{12}$$

The symbol g in (eq. 11) is the function which defines the Stribeck tire-road sliding friction (Andersson, Soderberg, & Bjorklund, 2007):

$$g(v_r, v_s) = \mu_C + (\mu_S - \mu_C)e^{-|v_r/v_s|^{0.5}} \tag{13}$$

where μ_C is the normalized Coulomb friction, μ_S is the normalized static friction ($\mu_C \leq \mu_S$, $\in$ [0, 1]) and v_s is the Stribeck relative velocity, all of which are physical characteristics observed upon contact between the tire rubber and runway asphalt materials. Stribeck velocity v_s is a boundary value of relative velocity at which surfaces stop sticking to one another and begin to slide relative to one another (Wojewoda, Stefanski, Wiercigroch, & Kapitaniak, 2008).

Dynamic stiffness and damping properties for the tire material are included to measure the tire/road friction force applied on the ground across the entire contact patch over time:

$$F_x = \left(\sigma_0\tilde{z} + \sigma_1\frac{d\tilde{z}}{dt} + \sigma_2 v_r\right)F_R \tag{14}$$

Where σ_1 is the normalized tire damping, and σ_2 is the normalized tire viscous friction. Combining equations (9) and (14), the friction coefficient can be expressed with:

$$\mu = \left(\sigma_0\tilde{z} + \sigma_1\frac{d\tilde{z}}{dt} + \sigma_2 v_r\right) \tag{15}$$

Suitable LuGre tire model parameters for the rubber used in aircraft tires are given in Table 1 (Li & Jiao, 2013).

Table 1
LuGre tire model parameters.

Name	σ_0	σ_1	σ_2	μ_C	μ_S	v_s
Value	1	0.1487	0.0038	0.5	0.9	12.5
Units	1/m	s/m	s/m	-	-	m/s

Inspection of (eq. 15) and Table 1 entails that the friction between tire and runway surface are strongly dependent upon the internal friction state and stretching of rubber within the tire contact patch. Friction coefficient with relative slip ratio λ is shown in Figure 3 for the tire model described above.

Figure 3 shows that the friction coefficient varies most rapidly between slip ratios of zero to 0.1 where a maximum is observed. Beyond the peak friction value, the amount of tractive friction force available decreases with increasing slip and the tire becomes less effective at providing traction.

Wheel Inertia

The wheel moment of inertia consists of two components, the tire and rim moments of inertia, as in (Day, 2014):

$$I = I_t + I_r \tag{16}$$

where I_t and I_r are the tire and rim moments of inertia, respectively. The tire can be assumed to be a circular ring; therefore its moment of inertia, $\mathrm{I_t}$ (circular ring) is:

$$I_t = m_t R^2 \tag{17}$$

where $\mathrm{m_t}$ represents the tire mass and R is its radius. The other wheel part is the rim, which can be approximated as two parts, a flat circular plate, and a circular ring. The mass of the flat plate is assumed equal to that of the circular ring. Therefore the rim moment of inertia is:

$$I_r = I_{r(circular)} + I_{r(flat)} \tag{18}$$

DOI: https://doi.org/10.15394/ijaaa.2015.1043

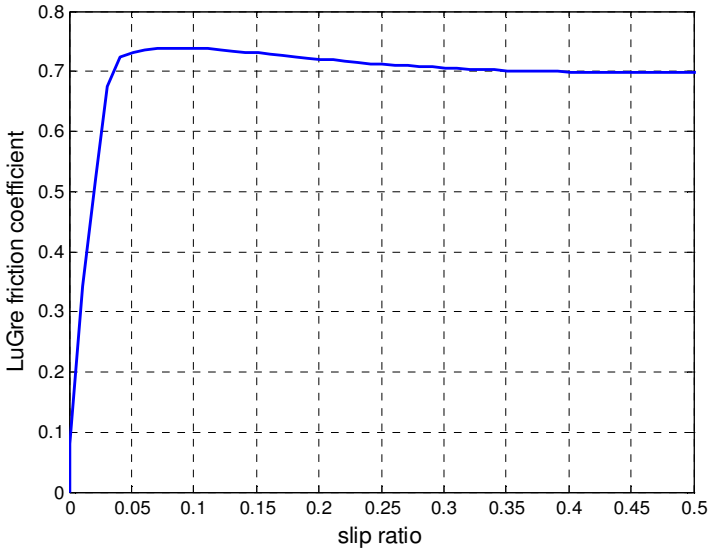

Figure 3. Friction coefficient μ between tire and runway with slip ratio λ from the LuGre model.

The rim circular ring moment of inertia is:

$$I_{r(circuar)} = (\frac{m_r}{2})\, {r_r}^2 \tag{19}$$

where m_r is the rim mass and r_r is its radius. The moment of the flat plate is:

$$I_{r(flat)} = \frac{(\frac{m_r}{2})\, {r_r}^2}{2} \tag{20}$$

Main landing gear wheel data are shown in Table 2 (Lufthansa Technik), and (Goodyear, 2002).

Table 2
Tire and rim data.

	Weight (Kg)	Radius (m)
Tire	110	0.622
Rim	74.4	0.255

The wheel inertia calculated from equations (16-20) and data in Table 2 is 46.2 kgm^2 and is used in (eq. 21).

Wheel Rotational Dynamics

The friction force F_X (eq. 14) acts at the tire contact patch, distanced from the wheel's axle by the effective radius. Utilising the rotational form of Newton's 2nd law, rotational acceleration of the wheel is:

$$\dot{\omega} = F_x r_e / I \tag{21}$$

where $\dot{\omega}$ is the wheel acceleration (rad/s^2), and r_e is the effective radius of the wheel under the immediate loading conditions.

Wheel speed with time is simply calculated as the integral of (eq. 21) with respect to time, plus an initial wheel speed:

$$\omega = \int \dot{\omega}\, dt + \omega_{init} \tag{22}$$

Where, ω is the wheel speed (rad/s), and ω_{init} is the wheel speed prior to touchdown.

Aircraft Landing Path and Speed

Figure 4 shows the aircraft flight path at approach, flare, touchdown, skidding, and deceleration. As shown in the Figure, the aircraft wheel will skid during the spin up (rotation phase) to reach free rolling, at which point the brakes will become effective.

The typical aircraft approach technique is to maintain a fixed speed to arrive 50 feet (15 m) over the runway threshold, before the flare manoeuvre. The flare is used to reduce vertical speed and conduct a smooth touchdown and to reduce the landing roll distance.

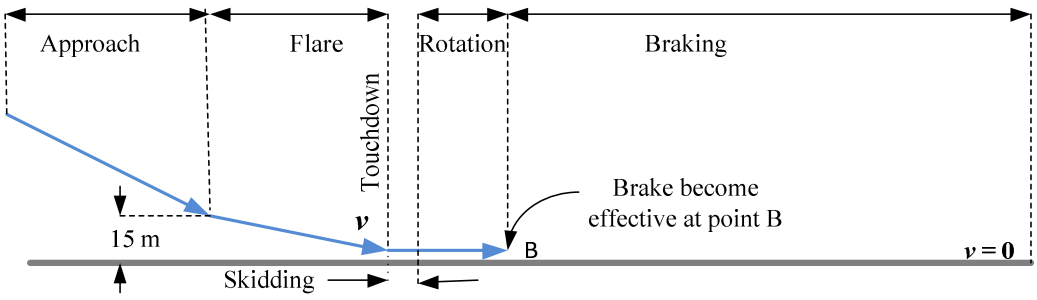

Figure 4. Typical Aircraft Landing Process (not to scale). Modified from Mair & Birdsall, 1992.

During the flare manoeuvre the vertical speed is variable, with pitch angle increased to induce drag and decelerate the aircraft by roughly 10 knots

DOI: https://doi.org/10.15394/ijaaa.2015.1043

(Ochi & Kanai, 1999). Li and Jiao (2013) states that the vertical sink rate at the instant of touchdown for the Boeing 747-400 aircraft typically varies between 1.5 m/s and 3 m/s.

A sink rate of 2 m/s is used at the start of each landing simulation in this study, and horizontal speed at touchdown speed is equal to the approach speed from Boeing (2011), 80.78 m/s, minus 5.14 m/s from flare deceleration (Ochi & Kanai, 1999), resulting in a horizontal touchdown speed of 75.6 m/s. That horizontal speed is assumed constant for the entire simulation, which is small and within the assumed two-second period before the pilot applies the brakes.

Tire Wear

The primary location of the abrasive action between tire and pavement during vehicle operation is on a thin layer of rubber in the tread immediately in contact with the road, called the footprint. This layer and the underlying belt layers are cyclically compressed and uncompressed, creating shear stresses and strains. These stresses and strains make up the frictional work between surfaces, which in turn causes wear of the tread. The magnitude of tread erosion is a function of the intensity and duration of the frictional work, the nature of the pavement, properties of the rubber, and other environmental factors (Li & Jiao, 2013).

Different methods independently attempt to quantify tire wear by isolating all but a few factors. The method by (Saibel & Tsai, 1969), aggregating abrasion pattern, slippage, and temperature effects, fatigue theory and the geometry of the contact surface. Other methods, such as Pacejka's "Magic Formula" (Braghin, Cheli, Melzi, & Resta, 2006) uses laboratory observed data to determine constants that best fit tire wear models. Pacejka's series of tire design models were named "magic" because they are not formed on any physical basis, but fit a wide array of construction and operating conditions.

The Archard wear theory is a simple model used to associate tire wear with slip, and is based around the theory of asperity contact. The calculation of adhesive wear is proposed by Archard (Zglimbea, Finca, Greaban, & Constantin, 2009), (Li, Zhang, & Guan, 2012), (Zhang, Zhang, & Yu, 2012), and (Tong, Wang & Jin, 2012).

The volume of tire material eroded in Archard wear theory is defined as:

$$V = K\frac{F_R}{H}L \tag{23}$$

where V represents the total volume of wear amount (m^3), K is the wear coefficient, F_R is the normal load applied to the tire contact patch (eq. 2), H is the hardness of the softer material in the contact (in our case the tire rubber), and L is the slip distance.

In the process of tire rolling, the slip distance can be defined as the integral of slip ratio from (eq. 10) with respect to time:

$$L = \int \lambda \, dt. \tag{24}$$

The rate of volume wear is then described as:

$$\dot{V} = K \frac{F_R}{H} \lambda \tag{25}$$

Where $\dot{V}$ is the tire wear volumetric rate (m^3/s). Because K and H are constants in the simple Archard model, the rate of volumetric tire wear is directly proportional to the product normal force and slip ratio or relative slipping velocity between the two contact materials. The inclusion of normal force implies that tire wear will scale linearly with aircraft mass. This implies that tire wear is roughly proportional to the amount of frictional work (force × slipping distance) at slip ratios above the peak in Figure 3; where μ is practically constant, which is also reported to be a reasonable in (Tong, & Jin, 2012), and (Lupker, Montanaro, Donadio, Gelosa, & Vis, 2002).

Eliminating the constants K and H, a "normalized wear" measure can be used to measure the relative difference in wear between landing simulations using different initial conditions without needing the material properties used in a calculation of volumetric wear. This normalized wear factor simply eliminates the constant wear coefficient and material hardness K and H from (eq. 25) to consider only the varying normal force and slip ratio. Normalized wear volume (Ns) is then simply:

$$V_N = \int (F_R \cdot \lambda) \, dt. \tag{26}$$

Normalised wear volume expressed in (eq. 26) is analogous to the "slip work" measure used in (Padovan, Kazempour & Kim, 1990), and was used in that study to represent the amount of tire wear between simulations and physical measurements.

Simulation Model Details

A schematic of calculation flow in the simulation model is presented in Figure 5. Computation begins with calculation of the vertical landing gear dynamics in equations (1-2), initialized with a non-zero starting sink rate $\dot{z}$ and

DOI: https://doi.org/10.15394/ijaaa.2015.1043

zero landing-gear strut compression z. Vertical acceleration $\ddot{z}$ is then integrated with respect to time to obtain the vertical speed $\dot{z}$ for the following time step.

Vertical force reacted at the tire contact with the ground is calculated with (eq. 2), and is used in the calculation of vertical tire deflection (eq. 3) and rolling radius (eq. 8). Wheel slip-ratio (eq. 10) is then computed using an initial wheel rotational speed and horizontal speed of the aircraft along the runway.

Slip ratio and vertical tire-load are used in the calculation of Normalized Archard wear volume (eq. 26) and in the calculation of longitudinal friction force F_X acting between the tire contact patch and runway surface (eq. 14).

The product of tire friction force F_X and instantaneous rolling radius is divided by wheel inertia to determine the rate of rotational acceleration of the wheel $\dot{\omega}$ (eq. 21). The time integral of wheel rotational acceleration is accumulated with (eq. 22) to obtain wheel speed in the following time step, which feeds back into the wheel slip calculation. In a post-processing step, the history of normalized Archard wear volumes for each time step are accumulated to obtain the total wear observed over a landing simulation.

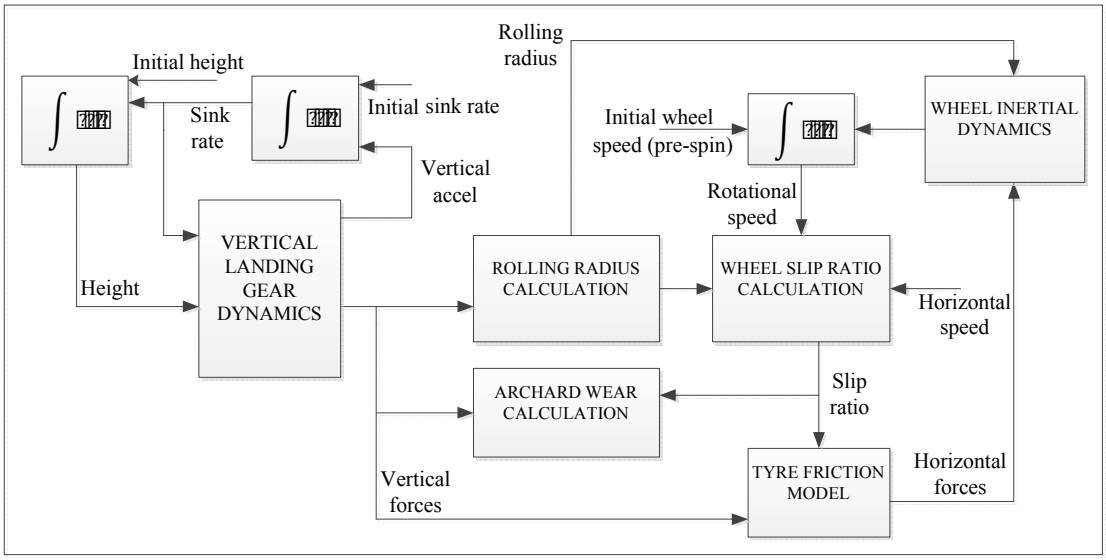

Figure 5. Schematic of calculation flow in simulation model.

The model described above was implemented with a model developed in Simulink, which is a data flow graphical programming language tool for modeling, simulating and analyzing dynamic systems. Ordinary-differential

equations in the model were solved using the Runge-Kutta Dormand-Prince (RKDP) method. A variable time-step was allowed between limits of $1x10^{-6}$ and $1x10^{-3}$ seconds, where the time step is reduced automatically if absolute and relative errors exceed a tolerance of $1x10^{-3}$ units.

The model was initiated with initial sink rate of 2 m/s and horizontal speed of 75.6 m/s for baseline calculations, and later the initial sink rates and vertical speeds where altered to allow the sensitivity of tire wear to initial aircraft speed to be estimated. For each set of initial vertical and horizontal aircraft speeds, a range of individual simulations were performed with various initial wheel rotational speeds at touchdown, to investigate potential improvements on tire wear from technologies that pre-spin an aircraft tire before touchdown. Vehicle mass was set to 295,743 kg (Boeing, 2011) for the simulations, with the vertical force on one tire being F_R from (eq. 2). Longitudinal tire force was initialized with a value of zero, and was accumulated with the tire dynamics described by the LuGre model above.

Simulation Results

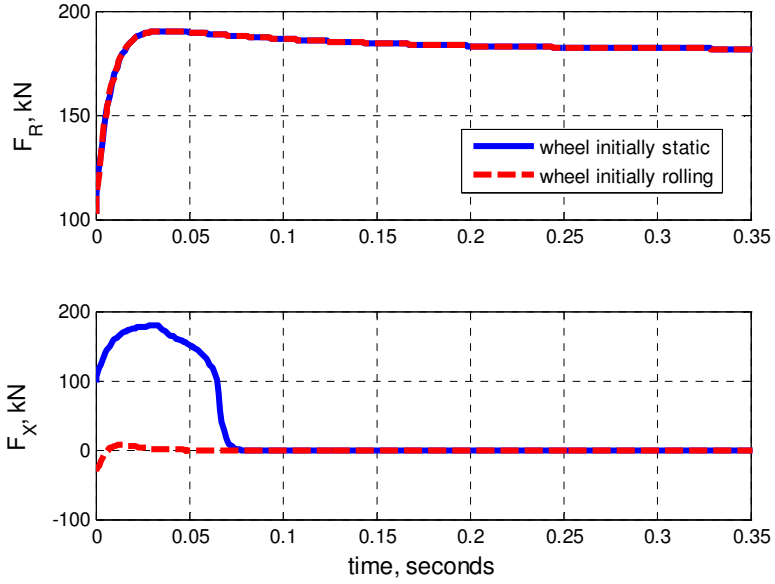

Figure 6. Vertical and longitudinal forces reacted at a single wheel contact patch during landing (initial sink rate = 2m/s, initial horizontal speed 75.6 m/s).

DOI: https://doi.org/10.15394/ijaaa.2015.1043

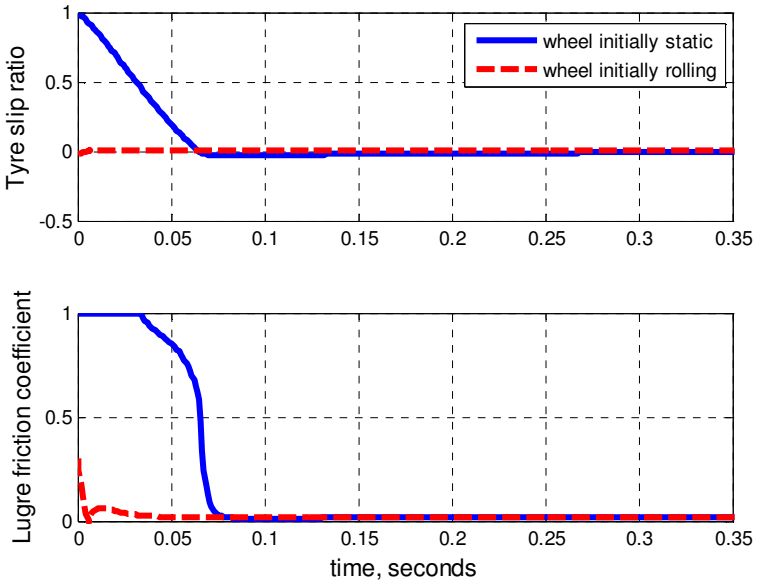

Figure 7. Slip ratio and dynamic friction coefficient during landing (initial sink rate = 2m/s, initial horizontal speed 75.6 m/s).

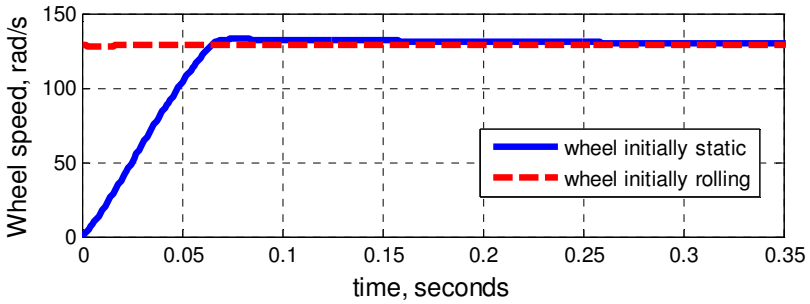

Figure 8. Rotational wheel speed with time during a landing (initial sink rate = 2m/s, initial horizontal speed 75.6 m/s).

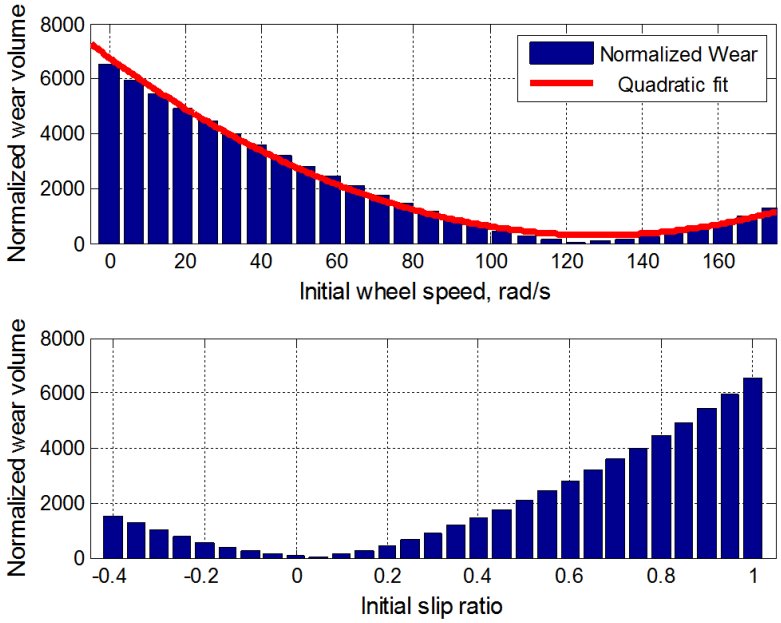

Figure 9. Normalized wear volume (eq. 26), with various wheel speeds at touchdown (slip ratio = 0 at 128.9 rad/s).

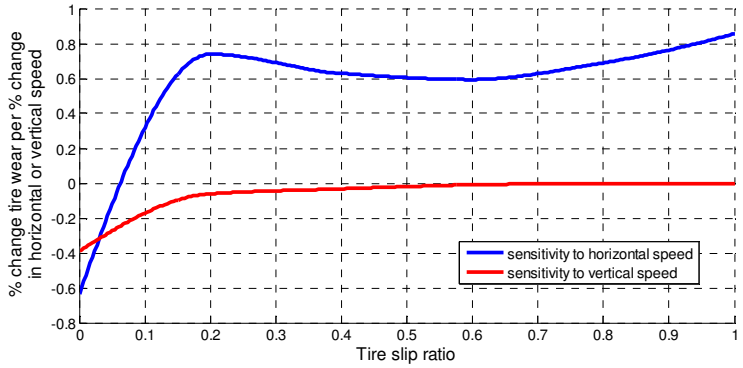

Figure 10. Sensitivity of tire wear volume to variations in initial horizontal aircraft speed and sink rate, plotted against initial wheel slip ratio.

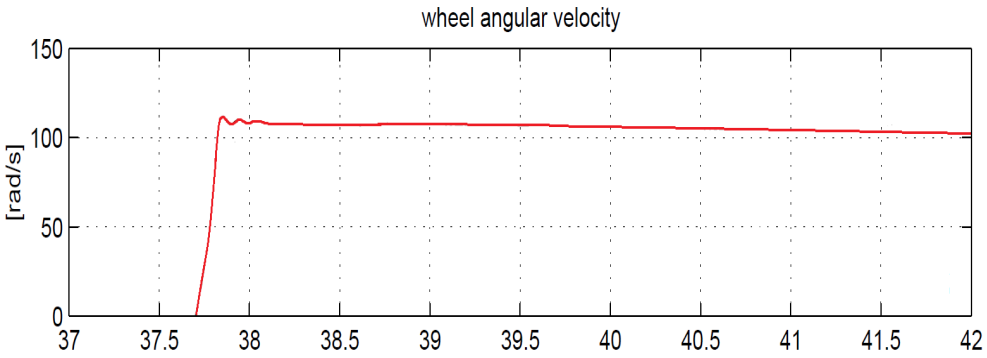

Figure 11. Measured wheel speed with tire that was static prior to touchdown, from Besselink, 2000.

Table 3
Normalized wear volumes (eq. 26) from separate simulations with 2 m/s sink rate and varied horizontal initial touchdown speed.

		Horizontal speed at touchdown, m/s						
		75.6	79.4	83.2	86.9	90.7	94.5	98.3
Initial Slip Ratio	0.00	70	68	65	63	62	60	58
	0.10	147	149	150	152	154	156	158
	0.20	432	448	464	479	495	510	525
	0.30	890	922	952	982	1011	1039	1067
	0.40	1454	1500	1545	1589	1631	1672	1712
	0.50	2094	2157	2217	2277	2335	2392	2449
	0.60	2804	2887	2968	3048	3128	3209	3289
	0.70	3589	3698	3807	3917	4028	4142	4257
	0.80	4459	4604	4752	4904	5061	5223	5390
	0.90	5431	5627	5829	6039	6257	6481	6711
	1.00	6528	6790	7062	7342	7628	7918	8209

Table 4
Normalized wear volumes (eq. 26) from separate simulations with 75.6 m/s horizontal touchdown speed and varied sink rate at touchdown.

		Vertical sink rate at touchdown, m/s						
		2	2.1	2.2	2.3	2.4	2.5	2.6
Initial Slip Ratio	0.00	70	69	67	66	65	63	62
	0.10	147	146	145	144	143	142	141
	0.20	432	431	430	428	427	426	425
	0.30	890	888	886	884	882	880	878
	0.40	1454	1452	1449	1447	1445	1443	1441
	0.50	2094	2092	2091	2089	2087	2085	2084
	0.60	2804	2803	2802	2801	2800	2799	2798
	0.70	3589	3588	3588	3587	3587	3586	3586
	0.80	4459	4459	4458	4458	4458	4458	4458
	0.90	5431	5431	5431	5430	5430	5430	5430
	1.00	6528	6526	6525	6524	6523	6522	6522

Discussion

Although simulations where performed for the period up to two seconds following aircraft touch-down, slowest settling variable (vertical load) reaches a steady state after just 0.35 seconds, and Figures 6-8 show the interesting part of the simulation timeframe.

Inspection of the blue lines for friction coefficient and wheel speed in Figures 7 & 8 show the friction coefficient is saturated at a maximum value of 1.0 up until 0.04 seconds, after which the wheel accelerates at an almost constant rate until $t = 0.07$ seconds in Figure 8. The initial rapid acceleration is driven by two factors, the dominant one being the strong vertical force reacted by the tire whilst the sink rate of the aircraft is dampened by shock absorbers in the landing gear (eq. 2) and secondly the longitudinal friction caused by deformation inside the tire material within the tire contact patch (eq. 14). During the initial period of large vertical load and slip, the tire friction coefficient is at a limiting value of 1.0 from equations (13-15), and the tire is in a “traction-limited” slipping state.

As the initial sink rate of the aircraft is dampened to zero, the vertical force in Figure 6 decays to a steady state and tire acceleration is almost constant. Friction force acting on the tire decays with a falling slip ratio as the tire spins up to a free-rolling velocity.

DOI: https://doi.org/10.15394/ijaaa.2015.1043

Within 0.08 seconds after touchdown, the wheel has settled to a speed where the slip ratio is less than 0.1 after a small overshoot around 0.07 seconds. Eventually the wheel reaches a speed where $\omega r_e = v$, i.e. the tangential speed of a point on the tire surface matches the forward speed of the aircraft along the runway causing the slip ratio to be zero. At this point the wheel spin-up phase has ended and the tire is effectively rolling freely until a braking effort is applied to the wheel.

During the entire spin-up phase the tire is considered to be skidding because slip ratio is significantly larger than zero. The three phases of tire behavior identified above are depicted in Figure 12 below.

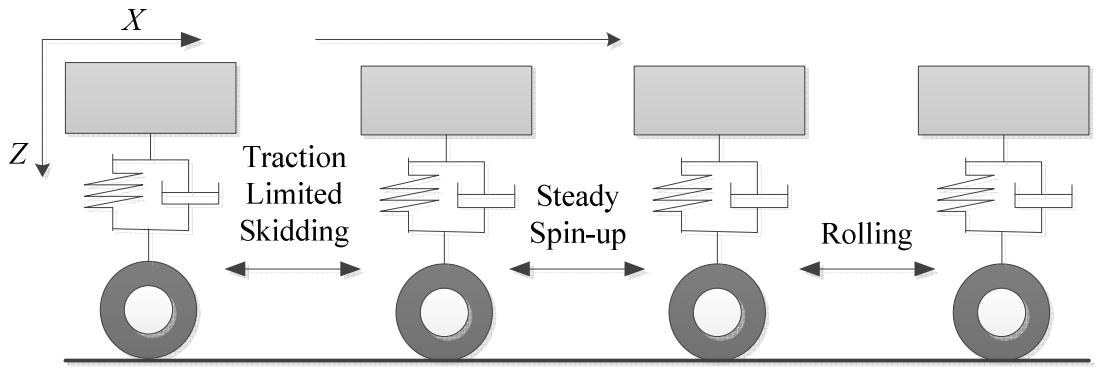

Figure 12. Wheel touchdown, skidding, spin-up, and rolling on the runway when the wheel is not spinning at the instant of touchdown.

In the simulation of a landing with the wheel already spinning at a speed to give zero slip (red plots in Figures 6-8); internal dynamic effects on tire forces from (eq. 14) invoke a highly damped oscillation in wheel speed. That oscillation ends when slip ratio returns to zero after 0.07 seconds. The small variations in tire speed would cause wear according to the Archard wear theory, although the volume of material worn from the tire would be just 1.07% of the wear observed in the simulation that began with a static wheel.

Figure 9 shows that normalized wear volume from a number of simulations with different initial wheel speeds. The wear volume is approximated well with a quadratic curve fit. The smallest amounts of wear is observed when the initial slip ratio is zero, and wear increases with the square of initial difference between aircraft forward speed and the linear velocity of a point on the outer radius of the tire. This implies that the wear in landing gear tires is proportional to the kinetic energy needed to spin a tire up to a rolling state.

Sensitivity analysis was performed by varying initial sink rate and horizontal speed in 5% increments up to 30% larger than the base values of 2 m/s and 75.6 m/s respectively. Results from sensitivity analysis on the data in tables 3 & 4 are shown in Figure 10, Tire wear is more sensitive to increases in aircraft horizontal speed than it is sensitive to increases in the vertical sink rate at touchdown. A one-percent increase in horizontal speed at touchdown is expected to increase tire wear by between 0.59% and 0.83% at slip ratios greater than 0.2. At lower initial slip ratios the sensitivity of tire wear to horizontal landing speed reduces.

When the wheel is already spinning at the free-rolling speed, at an initial slip ratio of zero, simulations showed tire wear actually reducing by 0.6% for every one-percent increase in landing speed, although the wear volume at such slip ratios is already very small so change in wear volume at zero slip in cubic metre s is practically negligible. Sensitivity to touchdown is about zero for initial slip ratios of 0.6 and above, and nonzero although practically negligible at lower slip ratios when a tangible measure of wear volume is considered. Slightly *negative* values of tire wear sensitivity to sink rate imply that heavier landings make the tire spin-up process more efficient, with *larger* vertical forces increasing the spin-up torque compared to more gentle touchdowns.

Figure 11 shows the tire speed with time from an experimental test performed on a Boeing 747-400 aircraft from (Besselink, 2000). The spin-up time of ~ 0.1 seconds corresponds well with our simulation, although the oscillation in wheel speed seen in the data was not present in our simulation results (Figure 8). It is expected that the flexible aircraft body is responsible for variations in tire vertical loading after touchdown, which would vary the friction force F_x acting on the tire, and is a second-order effect not captured by our lumped-mass vertical dynamics model.

Conclusions

A simulation model has been developed for comparing tire wear between an initially non-spinning aircraft main-gear wheel and a wheel that is already spinning at the instant of touchdown. A tire that is pre-spun to match the forward speed of the aircraft prior to touchdown will typically experience just 1.07% of the material removal from abrasive wear that would take place on an un-spun tire.

Tire wear increases by less than per one-percent increase in aircraft horizontal speed for un-spun tires. If a pre-spinning device is used to make the touchdown wheel slip ratio smaller than 0.2, sensitivity to longitudinal speed reduces. Tire wear is barely affected by touchdown sink rate in comparison to variations in horizontal speed.

DOI: https://doi.org/10.15394/ijaaa.2015.1043

Simplification of the Archard wear (eq. 23) to a normalized wear volume (eq. 26) allowed a relative comparison of tire wear between separate simulations to be made, without the need for tire or runway material properties. From simulating landings with a variety of initial wheel rotational speeds, Archard wear theory predicts that the amount of material worn from the tire on each landing is proportional to the square of the speed difference between aircraft forward speed and the tangential speed of a point on the tire tread at the instant of touchdown, i.e. the kinetic energy that the wheel must gain in order to reach a free-rolling state with zero slip. If the wheel was pre-spun to the free-rolling speed before the moment of touchdown, Archard wear theory predicts that tire wear would be reduced and therefore tire life could be improved significantly.

Future Work

The work performed in this study strongly suggests that a wheel spin-up device can improve the life of heavy aircraft main landing gear tires. Additional research should pursue the feasibility in terms of mechanical complexity and financial costs and benefits of implementing pre-spinning technologies on commercial aircraft. Simulation of the technologies highlighted in the literature review would be useful in identifying the characteristics of a pre-opening device that performs most effectively.

The Archard wear theory used to compare tire wear is a very simple linear approximation, and it would be advisable to compare with more other wear models to confirm the relative wear prediction from simulations between un-spun and pre-spun tires.

Only longitudinal dynamics where included in the case study presented in this paper. A further study could include the tire wear induced with initial lateral slip as well as longitudinal slip for cross-wind landings, although quantifying the distribution of crosswind component over a large number of landing events would be difficult. The cosine component of tire forces in crosswind landings would be interesting to add to the model, although it is expected that the tire wear component from this would be small.

References

Andersson, S., Soderberg, A., & Bjorklund, S. (2007). Friction models for sliding dry, boundary and mixed lubricated contacts. *Elsevier: Tribology International, 40*(4), 580-587. doi:10.1016/j.triboint.2005.11.014

Bartram, M., Mavros, G., & Biggs, S. (2010). A study on the effect of road friction on driveline vibrations. *Proceedings of the Institution of Mechanical Engineers, Part K: Journal of Multi-body Dynamics*, *224*(4), 321-340. doi: 10.1243/14644193jmbd266

Beazley, R. H. (1947). Aircraft wheel spinner and control. *U.S. Patent, Publication No. US2414849 A. Washington, DC: U.S. Patent and Trademark Office*. Retrieved from http://www.google.com/patents/US2414849

Besselink, I.J.M. (2000). Shimmy of aircraft main landing gears. *Delft: Technische Universiteit Delft. PhD thesis.* Retrieved from http://www.tue.nl/en/publication/ep/p/d/ep-uid/227775/

Boeing Commercial Airplane Co. (2011). *Approach speeds for Boeing airplanes*. Retrieved from http://www.boeing.com/assets/pdf/commercial/airports/faqs/arcandapproachspeeds.pdf

Braghin, F. Cheli, F., Melzi, S., & Resta, F. (2006). Tire wear model: validation and sensitivity analysis. *Springer:Meccanica, 41*(2)143-156. doi: 10.1007/s11012-005-1058-9

Cadle, S.H. & Williams, R.L. (1978). Gas and particle emissions from automobile tires in laboratory and field studies. *Taylor & Francis: Journal of the Air Pollution Control Association*, *28*(5), 502-507. doi: 10.1080/00022470.1978.10470623

Canudas-de-Wit, C., Petersen, M. L., & Shiriaev, A. (2003). A new nonlinear observer for tire/road distributed contact friction. *42nd IEEE International Conference on Decision and Control (IEEE Cat. No.03CH37475).* doi: 10.1109/CDC.2003.1272952

Canudas-de-Wit, C., Tsiotras, P., Velenis, E., Basset, M. & Gissinger, G. (2003). Dynamic friction models for road/tire longitudinal interaction. *Vehicle System*, *39*(3),189-226. doi: 10.1076/vesd.39.3.189.14152

DOI: https://doi.org/10.15394/ijaaa.2015.1043

Dahl, P. R. (1968). A solid friction model. *The Aerospace Corporation. Technical report.* Los Angeles: Los Angeles Air Force Station. Retrieved from www.dtic.mil/dtic/tr/fulltext/u2/a041920.pdf

Daidzic, N. E., & Shrestha, J. (2008). Airplane landing performance on contaminated runways in adverse conditions. *Journal of Aircraft 45*(6), 2131-2144. doi: 10.2514/1.38056

Daugherty, R. H. (2003). *A study of the mechanical properties of modern radial aircraft tires*. Retrieved from http://citeseerx.ist.psu.edu/viewdoc/download?doi=10.1.1.74.1702&rp=re&type=pdf

Day, A. J. (2014). *Braking of road vehicles*. Portsmouth, UK: Butterworth Heinemann.

De, S. K., & White, J. R. (Eds.), (2001). Rubber technologist's handbook., Shrewsbury, UK: ISmithers Rapra Publishing.

ESDU 71025. (1995). Frictional and retarding forces on aircraft tyres. Part I: introduction. *The Royal Aeronautical Society, 1971 amended 1995. London: IHS Inc.*

FAA. (2004). Airplane Flying Handbook. FAA Handbooks series. *US Department of Transportation, Federal Aviation Administration*. Washington, DC: Author.

Goodyear. (2002). *Aircraft data tire book.* Akron, OH: The Goodyear Tire & Rubber Co.

Hamza, S. (2014). Sensitivity analysis of tire model micro-coefficients. *MascotNum Annual Conference, ETH Zurich (Switzerland).* Retrieved from http://www.ibk.ethz.ch/su/mascotnum2014/PhDStudentsDay/PhDAbstracts MN14_-_Hamza.pdf

Horvath, V. & Szoke, B. B. (2006). Airplane tire saver by protrusion air foils. *World Intellectual Property Organization. Patent, Publication No. WO/2006/130944.*

Hunter, J. R. (1997). *Simple things won't save the Earth*. Austin, TX: University of Texas Press.

Jingzhe, J. (2007). A mixed mode function – Boundary element method for very large floating structure – Water interaction systems excited by airplane landing impacts. *Doctoral thesis*, *Southampton University*.

Khal, S., & Khal, A. (2013). Apparatus for pre-rotating aircraft tires. *U.S. Patent, Publication No. US20130112809A1*.

Khapane, P. D. (2004). Simulation of aircraft landing gear dynamics using flexible multibody dynamics methods in SIMPACK. *Conference: ICAS, Yokohama, Japan*. Retrieved from http://icas.org/ICAS_ARCHIVE/ICAS2004/PAPERS/262.PDF

Lernbeiss, R. (2004). Simulation of the dynamic behavior of an aircraft landing gear during landing. *Simpack User Meeting, Vienna University of Technology*. Retrieved from http://www.simpack.com/fileadmin/simpack/doc/usermeeting04/um04_tu-wien-lernb.pdf

Li, F. & Jiao, Z. (2013). Robust control for aircraft anti-skid braking system based on dynamic tire/road friction force model. *Proceedings of the 2nd International Conference on Computer Science and Electronics Engineering (ICCSEE)*. doi:10.2991/iccsee.2013.409

Li, Y., Zhang, J., & Guan, X. (2012). Estimation of vehicle parameters and road friction using steering torque and wheel speeds. *WSEAS Transactions on Systems*. Retrieved from http://www.wseas.org/multimedia/journals/systems/2012/54-561.pdf

Lindsley, N. J., & Talekar, N. B. (2000). A tire model for air vehicle landing gear dynamics. *International ADAMS User Conference*. Retrieved from http://web.mscsoftware.com/support/library/conf/adams/na/2000/18_usaf_tire_landing_gear.pdf

Lufthansa Technik. (n.d.). *Aircraft tires: more than just rubber on steel*. Retrieved from http://www.lufthansa-technik.com/aircraft-tires

Lupker, H.A, Montanaro, F., Donadio, D., Gelosa, E., & Vis, M.A. (2002). Truck tire wear assessment and prediction. *7th International Symposium on Heavy Vehicle Weights & Dimensions*, *Delft, The Netherlands*. Retrieved from http://road-transport-technology.org/Proceedings/7%20%20ISHVWD/Truck%20Tyre%20Wear%20Assessment%20And%20Predicion%20-%20L%20upker.pdf

Mair, A. W., & Birdsall, D. L. (1992). *Aircraft performance*. Cambridge, UK: Cambridge University Press.

DOI: https://doi.org/10.15394/ijaaa.2015.1043

Milwitzky, B., Lindquist, D. C., & Potter, D. M. (1955). An experimental study of applied ground loads in landing. *National advisory committee for aeronautics, Langley aeronautical laboratory, Washington, DC*. Retrieved from http://hdl.handle.net/2060/19930092250

Ochi, Y., & Kanai, K. (1999). Automatic approach and landing for propulsion controlled aircraft by H∞ control. *Proceedings of the 1999 IEEE International Conference on Control Applications (Cat. No.99CH36328).* vol.2, pp.997-1002. doi: 10.1109/CCA.1999.800951

Padovan, J., Kazempour, A., & Kim, Y. H. (1990). Aircraft landing-induced tire spinup. *Journal of Aircraft, 28*(12), 849-854. doi: 10.2514/3.46108

Persson, B. (2006). Rubber friction: role of the flash temperature. *Journal of Physics: Condensed Matter*, *18*(32), 7789-7823. doi: 10.1088/0953-8984/18/32/025

Saibel, E., & Tsai, C. (1969). Tire wear model. *Interim Report*, *Issue 2. Carnegie Mellon University.* New York: Clearing house.

Slagmaat, V. M.T.P. (1992). Tire models in aircraft landing gear simulation. *VehicleSystem Dynamics*, *21*(sup001), 108-115. doi: 10.1080/00423119208970002

Tanyolac, T. & Yasarcan, H. (2011). A soft landing model and a mass spring damper based control heuristic. *Proceedings of The 29th International System Dynamics Conference*. Retrieved from http://www.systemdynamics.org/conferences/2011/proceed/papers/P1119.pdf

Tomita, H. (1964). Friction coefficients between tires and pavements surfaces. *Naval Civil Engineering Lab Port Hueneme Calif.*Retrieved from http://www.dtic.mil/cgibin/GetTRDoc?AD=AD0705987

Tong, G., & Jin, X. (2012). Study on the simulation of radial tire wear Characteristics. *WSEAS Transaction on Systems*, *11*(8), 419-429. Retrieved from http://www.wseas.org/multimedia/journals/systems/2012/56-433.pdf

Tong, G., Wang, Q., & Jin, X. (2012). Adaptive lane keeping control of vehicles with tire influence. *International journal of Advancements in Computing Technology*, *4*(18), 433-440. doi:10.4156/ijact.vol4.issue18.51

United States Air Force (2007). *Republic F-84 Thunderjet pilot's flight operating manual*. Los Angeles: Periscope Film.

Wojewoda, J., Stefanski, A., Wiercigroch, M., & Kapitaniak, T. (2008). Hysteretic effects of dry friction: modelling and experimental studies. *Philosophical Transactions of the Royal Society A: Mathematical, Physical and Engineering Sciences*, *366*(1866), 747-765. doi:10.1098/rsta.2007.2125

Zglimbea, R., Finca, V., Greaban, E., & Constantin, M. (2009). Research on parameter identification of modified friction LuGre Model based distributions theory. *WSEAS Transactions on Systems*, *8*(8), 978-987. Retrieved from http://www.wseas.us/e-library/transactions/systems/2009/29-647.pdf

Zhang, Y., Zhang, G., & Yu, F. (2012). Modeling and μ synthesis control of vehicle active suspension with motor actuator. *WSEAS Transactions on Systems*, *11*(5), 173-186. Retrieved from http://www.wseas.org/multimedia/journals/systems/2012/55-235.pdf

DOI: https://doi.org/10.15394/ijaaa.2015.1043